
Diffusion-C: Unveiling the Generative Challenges of Diffusion Models through Corrupted Data

Keywoong Bae^{1,2*} Suan Lee³ Wookey Lee^{1†}

¹Inha University ²POSTECH ³Semyung University

kwbae@postech.ac.kr; suanlee@semyung.ac.kr; trinity@inha.edu;

Abstract

In our contemporary academic inquiry, we present "Diffusion-C," a foundational methodology to analyze the generative restrictions of Diffusion Models, particularly those akin to GANs, DDPM, and DDIM. By employing input visual data that has been subjected to a myriad of corruption modalities and intensities, we elucidate the performance characteristics of those Diffusion Models. The noise component takes center stage in our analysis, hypothesized to be a pivotal element influencing the mechanics of deep learning systems. In our rigorous expedition utilizing Diffusion-C, we have discerned the following critical observations: **(I)** Within the milieu of generative models under the Diffusion taxonomy, DDPM emerges as a paragon, consistently exhibiting superior performance metrics. **(II)** Within the vast spectrum of corruption frameworks, the fog and fractal corruptions notably undermine the functional robustness of both DDPM and DDIM. **(III)** The vulnerability of Diffusion Models to these particular corruptions is significantly influenced by topological and statistical similarities, particularly concerning the alignment between mean and variance. This scholarly work highlights Diffusion-C's core understandings regarding the impacts of various corruptions, setting the stage for future research endeavors in the realm of generative models.

1 Introduction

Deep learning models have shown remarkable performances in various domains but unlike human vision, they are fundamentally vulnerable to adversarial attacks and various corruptions[1–3]. Deep learning is significantly affected not only by substantial and critical noise but also by minor deformations. Numerous benchmarks exist to identify the different failure patterns of models when subjected to a range of corruptions[4, 5]. The Denoising Diffusion Probabilistic Model (DDPM)[6–8], which falls under the diffusion generative model category, has proven its prowess in creating top-tier images. Of late, DDPM has garnered significant attention, leading to numerous studies exploring its inherent boundaries. Although many studies have been conducted [9–12], only a handful have investigated the resilience of Diffusion Models in the context of vulnerability challenges.

Drawing from prior studies on the susceptibilities of Diffusion Models[13–19], this manuscript utilizes adversarial attack methodologies to probe the vulnerabilities inherent in Diffusion Models. By training Diffusion Models using various corruptions both in type and intensity as input, our objective is to determine the specific disturbances to which the generative models are susceptible and their respective magnitudes. For the purpose of this research, we've termed this approach of using adversarial attacks on Diffusion Models to evaluate how changes in input values influence output value shifts as **Diffusion-C**.

*Work started while being student at Inha University

†Corresponding author

2 Methodology

2.1 What is Diffusion-C?

Original Diffusion Model’s training mechanism consists of two processes, Diffusion and Denoising. In diffusion process, the original image (x_0) gradually transforms into a purely noisy sample (x_T) by being injected gaussian noises (β_t) incrementally. After then, DDPM returns the final image x_g as a result of denoising process, while DDIM samples from intermediate noisy versions $q(\tilde{x}_t|x_0, x_k)$ of the data and then denoises from there. If the state of x_g and x_0 is similar, we interpret it as a good return performance of the Diffusion Models on their generative ability.

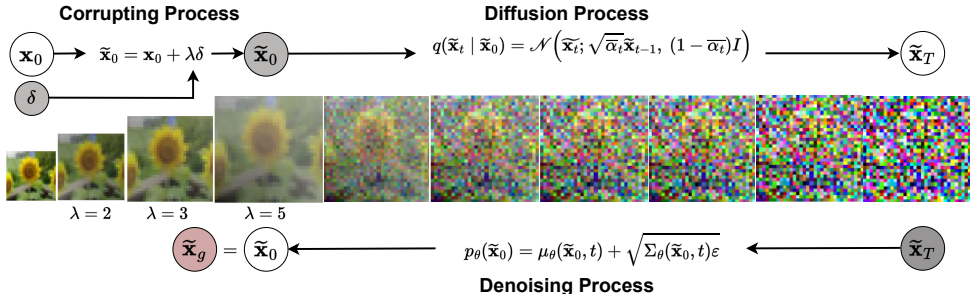


Figure 1: **Brief mechanism on Diffusion-C.** Unlike the mechanism of original Diffusion Models, Diffusion-C has a process of Corrupting. To summarize the generative limitations of Diffusion Models, we used corrupted images as an input and they were corrupted with various types and severities of corruption at corrupting process vice versa.

To observe the generative draws of Diffusion Models, we implemented a method of **Diffusion-C** through the following two stages of questions.

Q1) If the original initial input is corrupted with non-Gaussian noise (δ) instead of Gaussian noise (ϵ), can Diffusion Models still return quality images?

At first, we contemplated whether the return performance of Diffusion Models would still be good in the case of substituting original input (x_0) to corrupted input (x_t) with some Gaussian noise ($x_0 + \epsilon = x_t$). And this inquiry was expanded based on the recent researches on corruption benchmarks[4, 5] and various efforts for replacing Gaussian noise to non-Gaussian noise[20, 21]. We replaced Gaussian noise to non-Gaussian noise, which is defined as Corruptions in this work.

We aimed to observe the degradation of Diffusion Models’s return performance when $\tilde{x}_0 (= x_t + \delta)$ is used as an input instead of original x_0 . In 3.1, we compared the return performance of Diffusion Models with those of DCGAN[22] and WGAN-GP[23].

Q2) How far can Diffusion Models’s Return performance degrade?

This study primarily seeks to understand the boundaries of generative capabilities in Diffusion Models. By intensifying the corruption levels, we assessed the extent to which the performance of these models deteriorates. After finding a specific corruption δ , to which Diffusion Models are vulnerable, we observed how far Diffusion Models’s performance will degrade with respect to the severity (λ) of the corruption.

3 Experimental Results

The image datasets, originally with values between 0 and 255, were resized to fall between -1 and 1 for training. We utilized the Adam optimizer, set with a learning rate of 10^{-4} and a batch size of 128. We incrementally adjusted the Gaussian noise by 0.02, beginning at 10^{-4} . The model’s performance was gauged using the Fréchet Inception Distance (FID) [24]. This investigation sequentially built on the findings of each experiment, amplifying their significance, before advancing to the subsequent study.

3.1 Basic Comparison Experiments

In our research, our initial experiments were focused on (i) assessing the return performance of the generative model, and (ii) pinpointing its most critical vulnerabilities to corruptions. We made comparative evaluations using models like DDPM[6], DDIM[25], DCGAN[22], and WGAN-GP[23]. From the results, DDPM stood out as the top performer, followed by DDIM, WGAN-GP and DCGAN. On average, DDIM trained 730/56 times faster than DDPM, but the quality of the images it produced was slightly lower than DDPM. Moreover, of all the corruption types examined, Diffusion Models were particularly vulnerable to fog corruption.

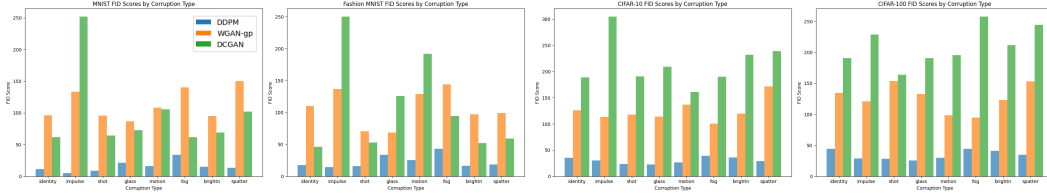


Figure 2: **Result of Fréchet Inception Distance score.** Blue is for DDPM, Orange for WGAN-GP, and Green for DCGAN.

Table 1: FID scores of DDPM/DDIM on the various corruptions

		Clear	Noise	Blur		Weather		Extra	
		Identity	Impulse	Shot	Glass	Motion	Brightness	Fog	Spatter
DDPM	MNIST	11.45	5.12	8.91	21.24	16.11	14.93	33.73	13.46
	Fashion MNIST	17.35	14.40	15.91	33.89	25.25	16.53	42.84	18.67
	CIFAR-10	33.53	30.38	23.56	22.39	26.27	35.91	39.23	29.02
	CIFAR-100	44.31	28.76	28.23	25.62	29.82	41.26	44.10	34.60
DDIM	CIFAR-100	70.16	52.33	67.35	61.23	56.88	68.55	71.63	65.60

3.2 Severity Experiments

Our subsequent experiment sought to understand how the severity of fog corruption influenced the top-performing model, DDPM’s return performance. We postulated that an escalation in corruption severity would result in a downturn in DDPM’s performance. Experimental designs incorporated five tiers of fog severity ($\lambda = 1 \sim 5$) across five datasets (including the previously mentioned four and Tiny-ImageNet-C[4]). Using the scenario with $\lambda = 1$ as a benchmark, we assessed the degree of performance degradation as severity fluctuated.

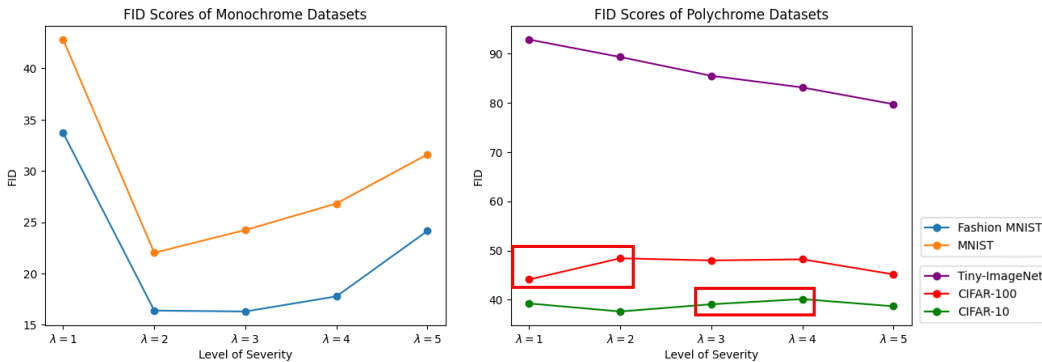


Figure 3: **The Variation in DDPM Performance with respect to Severity.** While fog corruption degrades the generative ability of DDPM, it doesn’t get worse as it gets stronger.

In datasets with monochrome imagery, FID scores were surprisingly better (lower) at heightened corruption levels relative to the baseline, suggesting that fog corruption might have inadvertently

aided DDPM in extracting features from monochrome images. For datasets with a broader color palette, no marked changes stood out. Minor deteriorations were observed at the initial shift in CIFAR-10 and the tertiary shift in CIFAR-100, though they were not of significant concern. While the intensity of fog severity appears to have a negligible effect on the Diffusion model’s generative output, it was discerned that DDPM and DDIM’s susceptibility to specific corruptions is notably shaped by topological and statistical congruences, especially the correspondence between mean and variance.

3.3 Fractal Independence Experiments

We delved deeper into the Fog corruption, rooted in the theoretical Plasma Fractal that showcases self-similarity traits and is generated via the Diamond-Square Algorithm[26]. Given the fog’s association with fractal designs, we hypothesized that DDPM and DDIM might encounter challenges when trained on images with fractal structures. To discern the notable generative constraints of DDPM and DDIM, we undertook an experiment employing the Fractal Dream dataset. This dataset is segmented into red, green, and blue image categories, each encompassing around 2,000 datasets at a resolution of 128×128 pixels. Before initiating training, we expanded this dataset using augmentation methods, amassing close to 22,000 samples.

Table 2: FID scores of DDPM on the Fractal Datasets

		Clear Identity	Noise		Blur		Weather		Extra Spatter
			Impulse	Shot	Glass	Motion	Brightness	Fog	
DDPM	Blue	21.76	9.64	11.90	15.93	14.19	21.86	24.52	23.55
	Red	26.16	14.96	9.86	13.98	22.63	23.96	26.19	18.67
	Green	33.53	30.38	23.56	22.39	26.27	35.91	39.23	29.02
DDIM	Red	95.73	69.05	65.56	85.54	129.46	98.74	99.66	120.71
	Green	80.67	58.51	39.90	51.67	77.39	78.76	88.62	89.20

Surprisingly, our results indicated that neither DDPM nor DDIM demonstrated significant vulnerability in generating images with fractal patterns. We divided our analysis into two distinct cases: initially, we superimposed fractal corruption onto the foundational image ($\tilde{x}_0 = x_0 + \delta$); subsequently, we considered images that intrinsically exhibited a fractal pattern (x_δ). From this assessment, it became evident that, in particular, the generative prowess of DDPM might be considerably undermined when exclusively confronted with corruptions of a fractal nature.

4 Discussion and Future works

This research is focused on unravelling the inherent limitations of generative models. Employing the Diffusion-C framework, we evaluated the model’s efficacy across an array of experimental conditions, leading us to three distinct conclusions (I, II, III). The trajectory of future research in this domain should address specific considerations: The enigmatic internal operations of deep learning often categorize it as a gray box, complicating our understanding of why generative models might be vulnerable to corruptions like the fractal one. In response, our approach has been to validate our propositions empirically by subjecting diffusion models to diverse environments. Furthermore, it’s worth addressing the metric concern. Generative models aim to generate ‘novelty’. However, as the FID predominantly measures similarity to existing data, there emerges a clear necessity for a new metric tailored to assess this element of novelty as well as corrupted ones.

References

- [1] Ian J Goodfellow, Jonathon Shlens, and Christian Szegedy. Explaining and harnessing adversarial examples. *arXiv preprint arXiv:1412.6572*, 2014.
- [2] Samuel Henrique Silva and Peyman Najafirad. Opportunities and challenges in deep learning adversarial robustness: A survey. *arXiv preprint arXiv:2007.00753*, 2020.
- [3] Wenye Liu, Si Wang, and Chip-Hong Chang. Vulnerability analysis on noise-injection based hardware attack on deep neural networks. In *2019 Asian Hardware Oriented Security and Trust Symposium, 1–6*. IEEE, 2019.
- [4] Dan Hendrycks and Thomas Dietterich. Benchmarking neural network robustness to common corruptions and perturbations. *arXiv preprint arXiv:1903.12261*, 2019.
- [5] Evgenia Rusak, Lukas Schott, Roland S. Zimmermann, Julian Bitterwolf, Oliver Bringmann, Matthias Bethge, and Wieland Brendel. A simple way to make neural networks robust against diverse image corruptions. In *ECCV, 53–69*, 2020.
- [6] Jonathan Ho, Ajay Jain, and Pieter Abbeel. Denoising diffusion probabilistic models. *Advances in Neural Information Processing Systems*, 33:6840–6851, 2020.
- [7] Hanqun Cao, Cheng Tan, Zhangyang Gao, Guangyong Chen, Pheng-Ann Heng, and Stan Z Li. A survey on generative diffusion model. *arXiv preprint arXiv:2209.02646*, 2022.
- [8] Florinel-Alin Croitoru, Vlad Hondru, Radu Tudor Ionescu, and Mubarak Shah. Diffusion models in vision: A survey. *IEEE Transactions on Pattern Analysis and Machine Intelligence*, 2023.
- [9] Cristiana Tiago, Sten Roar Snare, Jurica Sprem, and Kristin McLeod. A domain translation framework with an adversarial denoising diffusion model to generate synthetic datasets of echocardiography images. *IEEE Access*, 11:17594–17602, 2023.
- [10] Haomin Zhuang, Yihua Zhang, and Sijia Liu. A pilot study of query-free adversarial attack against stable diffusion. In *IEEE/CVF Conference on Computer Vision and Pattern Recognition*, 2385–2392. IEEE, 2023.
- [11] Boah Kim, Yujin Oh, and Jong Chul Ye. Diffusion adversarial representation learning for self-supervised vessel segmentation. In *ICLR*, 2023.
- [12] Shutong Wu, Jiong Xiao Wang, Wei Ping, Weili Nie, and Chaowei Xiao. Defending against adversarial audio via diffusion model. In *ICLR*, 2023.
- [13] Qinsheng Zhang, Molei Tao, and Yongxin Chen. gddim: Generalized denoising diffusion implicit models. In *ICLR*, 2023.
- [14] Gwanghyun Kim, Taesung Kwon, and Jong Chul Ye. Diffusionclip: Text-guided diffusion models for robust image manipulation. In *Proceedings of the IEEE/CVF Conference on Computer Vision and Pattern Recognition*, 2426–2435, 2022.
- [15] Cheng Lu, Yuhao Zhou, Fan Bao, Jianfei Chen, Chongxuan Li, and Jun Zhu. Dpm-solver: A fast ode solver for diffusion probabilistic model sampling in around 10 steps. *Advances in Neural Information Processing Systems*, 35:5775–5787, 2022.
- [16] Yunke Wang, Xiyu Wang, Anh-Dung Dinh, Bo Du, and Charles Xu. Learning to schedule in diffusion probabilistic models. In *Proceedings of the 29th ACM SIGKDD Conference on Knowledge Discovery and Data Mining*, 2478–2488, 2023.
- [17] Muiyang Li, Ji Lin, Chenlin Meng, Stefano Ermon, Song Han, and Jun-Yan Zhu. Efficient spatially sparse inference for conditional gans and diffusion models. *Advances in Neural Information Processing Systems*, 35:28858–28873, 2022.
- [18] Bram Wallace, Akash Gokul, and Nikhil Naik. Edict: Exact diffusion inversion via coupled transformations. In *Proceedings of the IEEE/CVF Conference on Computer Vision and Pattern Recognition*, 22532–22541, 2023.

- [19] Tomoya Matsumoto, Takayuki Miura, and Naoto Yanai. Membership inference attacks against diffusion models. *arXiv preprint arXiv:2302.03262*, 2023.
- [20] Eliya Nachmani, Robin San Roman, and Lior Wolf. Non gaussian denoising diffusion models. *arXiv preprint arXiv:2106.07582*, 2021.
- [21] Giannis Daras, Mauricio Delbracio, Hossein Talebi, Alex Dimakis, and Peyman Milanfar. Soft diffusion: Score matching with general corruptions. *Trans. Mach. Learn. Res.*, 2023.
- [22] Alec Radford, Luke Metz, and Soumith Chintala. Unsupervised representation learning with deep convolutional generative adversarial networks. *arXiv preprint arXiv:1511.06434*, 2015.
- [23] Ishaan Gulrajani, Faruk Ahmed, Martin Arjovsky, Vincent Dumoulin, and Aaron C Courville. Improved training of wasserstein gans. *Advances in neural information processing systems*, 30, 2017.
- [24] Martin Heusel, Hubert Ramsauer, Thomas Unterthiner, Bernhard Nessler, and Sepp Hochreiter. Gans trained by a two time-scale update rule converge to a local nash equilibrium. *Advances in neural information processing systems*, 30, 2017.
- [25] Jiaming Song, Chenlin Meng, and Stefano Ermon. Denoising diffusion implicit models. In *9th International Conference on Learning Representations, ICLR 2021*.
- [26] Alain Fournier, Don Fussell, and Loren Carpenter. Computer rendering of stochastic models. *Communications of the ACM*, 25(6):371–384, 1982.
- [27] Olaf Ronneberger, Philipp Fischer, and Thomas Brox. U-net: Convolutional networks for biomedical image segmentation. In *MICCAI, 234–241*. Springer, 2015.

Contents

1	Introduction	1
2	Methodology	2
2.1	What is Diffusion-C?	2
3	Experimental Results	2
3.1	Basic Comparison Experiments	3
3.2	Severity Experiments	3
3.3	Fractal Independence Experiments	4
4	Discussion and Future works	4
A	Introduction to Diffusion-C	8
A.1	Notations	8
A.2	How does Diffusion-C work?	8
B	Detailed Experimental Explanations	10
B.1	Basic Comparison Experiment	10
B.2	Severity Experiment	11
B.3	Fractal Independence Experiment	11

A Introduction to Diffusion-C

A.1 Notations

Table 3: Notations.

Notations	Description	Notations	Description
x	Non-corrupted observable data	\tilde{x}	Corrupted observable data
x_0	Original point of x	\tilde{x}_0	Original point of \tilde{x}
x_t	Diffused x_0 at time $t \in \{0, 1, \dots, T\}$	\tilde{x}_t	Diffused \tilde{x}_0 at time $t \in \{0, \dots, T\}$
x_T	Random noise after diffusing x_0	\tilde{x}_T	Random noise after diffusing \tilde{x}_0
x_g	Return point of x_0	\tilde{x}_g	Return point of \tilde{x}_0
t	Time index $t \in \{0, 1, \dots, T\}$	y	target data
D, G	Discriminator, Generator	θ, ϕ	learnable parameters
z	Random noise with normal distribution	$\mathcal{L}_D, \mathcal{L}_G$	Loss function of D and G
$D(G(z))$	$P(\text{real} \text{fake image})$	$D(x)$	$P(\text{real} \text{real image})$
L_0, L_{t-1}	Diffusion loss, denoising loss	L_T	Decoder loss
β_t	Variance scale coefficient	$\alpha_t, \bar{\alpha}_t$	$\alpha_t := 1 - \beta_t, \bar{\alpha}_t := \prod_{s=1}^t \alpha_s$
\mathcal{C}	Corruptions set	λ	Severity Level of Corruptions.
ϵ	Gaussian noise	δ_n	Each corruption for $\delta_k \in \mathcal{C}$
\mathcal{N}	Normal distribution	$\mathcal{F}, \tilde{\mathcal{F}}$	Similarity between (x_0, x_g) and $(\tilde{x}_0, \tilde{x}_g)$
$q(x_t x_{t-1})$	Diffusion process at time t	$p_\theta(x_{t-1} x_t)$	Denoising process at time $t - 1$
$\epsilon_\theta(x_t, t)$	Noise prediction model	$\Sigma_\theta(x_t, t)$	Variance coefficient of reversed step

A.2 How does Diffusion-C work?

Algorithm 1. Mechanism on Diffusion-C

```

1 : Input :  $x_0$ , Each corruptions :  $\delta_k (\delta_k \in \mathcal{C}), \epsilon \sim \mathcal{N}(0, I), \alpha_t := 1 - \beta_t$ 
2 : for  $\delta_k$  in  $\mathcal{C}$  do
3 :    $\tilde{x}_0 = x_0 + \lambda \delta_k$  ( $1 \leq \lambda \leq 5$ ) // (1) corruption process
4 :   repeat
5 :      $\tilde{x}_0 \sim q(\tilde{x}_0)$ 
6 :     Take gradient descent step on
7 :      $\nabla_\theta \|\epsilon - \epsilon_\theta(\sqrt{\bar{\alpha}_t} \tilde{x}_0 + \sqrt{1 - \bar{\alpha}_t} \epsilon, t)\|^2$ 
8 :     until converged // (2) diffusion process
9 :     for  $t = T, \dots, 1$  do
10 :       $\tilde{x}_{t-1} = \frac{1}{\sqrt{\alpha_t}} (\tilde{x}_t - \frac{1 - \alpha_t}{\sqrt{1 - \alpha_t}} \epsilon_\theta(\tilde{x}_t, t)) + \sigma_t z$ 
11 :     end for
12 :      $\tilde{x}_g = \int p(\tilde{x}_T) \prod_{t=1}^T p_\theta(\tilde{x}_{t-1} | \tilde{x}_t) d\tilde{x}_{1:T}$  // (3) denoising process
13 :   return  $\max(\mathcal{F}(\tilde{x}_0, \tilde{x}_g), \mathcal{F}(x_0, x_g))$ 
14 : end for

```

DDPM (Denoising Diffusion Probabilistic Models) [6–8] is a generative model that employs the Markov Chain Monte Carlo (MCMC) method to learn the underlying structure of a dataset and generate a class of latent variable models. The objective of Diffusion-C is also to minimize the negative log-likelihood (NLL) function, which can be formulated as a minimization problem.

$$\begin{aligned}
E[-\log p_\theta(\tilde{x}_0)] &\leq E_q[-\log \frac{p_\theta(\tilde{x}_{0:T})}{q(\tilde{x}_{1:T}|\tilde{x}_0)}] = E_q[-\log p(\tilde{x}_T) - \sum_{t \geq 1} \frac{p_\theta(\tilde{x}_{t-1}|x_t)}{q(\tilde{x}_t|\tilde{x}_{t-1})}] \\
&= D_{KL}(q(\tilde{x}_T|\tilde{x}_0)||p(\tilde{x}_T)) + \sum_{t > 1} D_{KL}(q(\tilde{x}_{t-1}|\tilde{x}_t, 0)||p_\theta(\tilde{x}_{t-1}|\tilde{x}_t, \tilde{x}_0)) \quad (1) \\
&- E_q[\log p_\theta(\tilde{x}_0|\tilde{x}_1)] = E_q[L_T + L_{t-1} + L_0] =: L.
\end{aligned}$$

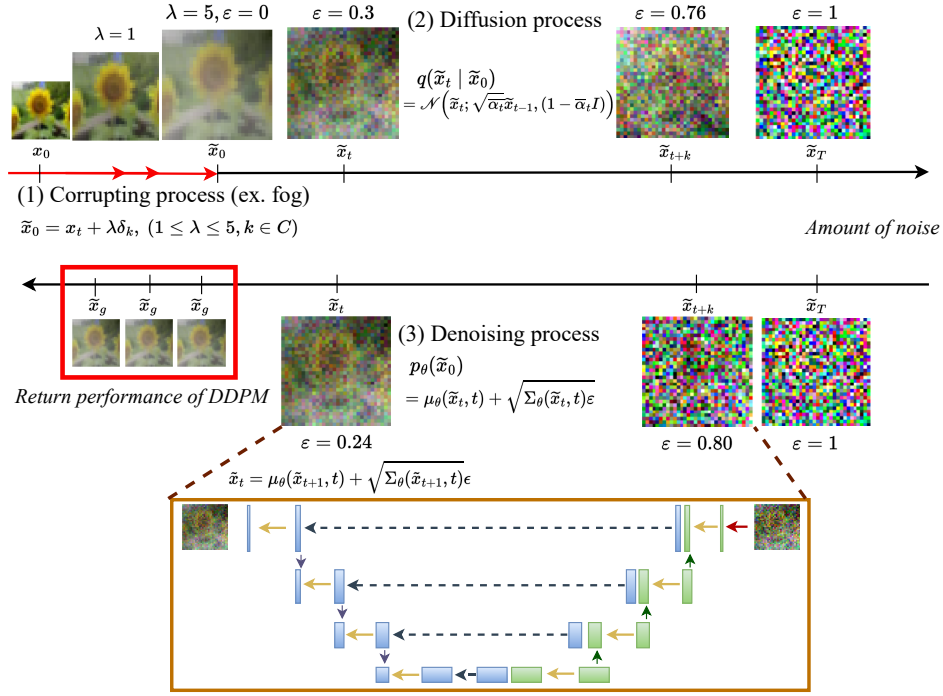


Figure 4: **Overall mechanism on Diffusion-C.** The training process of Diffusion-C consists of (1) Corrupting process, (2) Diffusion process and (3) Denoising process. For the denoising step, a U-Net[27] was used as the noise prediction network. After denoising process, Diffusion model returns final image \tilde{x}_g , which is the outcome of Diffusion-C. By calculating the differences between \tilde{x}_0 and \tilde{x}_g in various conditional experiments, we identified when the return performance of DDPM deteriorates the most.

Diffusion-C comprises of three stages: (1) Corrupting, (2) Diffusion, and (3) Denoising. Initially, the original dataset x_0 is corrupted into \tilde{x}_0 , which results in the disturbance of the original point's information. Starting from the new original state, \tilde{x}_0 is transformed into \tilde{x}_T through the diffusion process and eventually returns to \tilde{x}_g through the denoising process. The effectiveness of DDPM is determined by the degree of similarity between \tilde{x}_0 and \tilde{x}_g , denoted by the expression $\mathcal{F}(\tilde{x}_0, \tilde{x}_g)$.

(1) Corrupting Process (L_0). The corrupting process involves perturbing the original dataset with corruptions. Using various types and severities of corruptions, Diffusion-C transforms the original image into a corrupted one, \tilde{x}_0 .

$$\tilde{x}_0 = x_t + \lambda \delta_k \quad (0 \leq t \leq T, 1 \leq \lambda \leq 5, k \in C). \quad (2)$$

(2) Diffusion Process (L_T). The diffusion process involves repeatedly adding Gaussian noise (β_t) to the corrupted image \tilde{x}_t at every timestep t to create a noisy state \tilde{x}_T . The diffusion process of Diffusion-C can be represented as $q(\tilde{x}_{1:T} | \tilde{x}_0)$.

$$q(\tilde{x}_t | \tilde{x}_0) = \mathcal{N}(\tilde{x}_t; \sqrt{\bar{\alpha}_t} \tilde{x}_0, (1 - \bar{\alpha}_t)I). \quad (3)$$

(3) Denoising Process ($L_{1:T-1}$). DDPM trains the denoising process to move \tilde{x}_T back to the original state of \tilde{x}_0 . In this process, the noise injected into the image is removed to reveal the original state. It is represented by $p_\theta(\tilde{x}_{0:T}) := p(\tilde{x}_T) \prod_{t=1}^T p_\theta(\tilde{x}_{t-1} | \tilde{x}_t)$, and the denoising process at time t can be expressed as follows.

$$p_\theta(\tilde{x}_{t-1} | \tilde{x}_t) := N(\tilde{x}_{t-1}; \mu_\theta(\tilde{x}_t), \Sigma_\theta(\tilde{x}_t, t)). \quad (4)$$

p_θ is used to learn the process of removing the noise based on q which learns $\mu_\theta(\tilde{x}_t, t)$ and $\Sigma_\theta(\tilde{x}_t, t)$.

B Detailed Experimental Explanations

B.1 Basic Comparison Experiment

Type of Corruptions. In this experiment, we used total seven corruptions. Shot noise is the Poisson noise, and Impulse noise is the salt-pepper noise. Glass blur simulates noises through glass by mixing pixels. Motion blur is the corruption blurring the image along any line. Brightness is made with the increment of images. Fog simulates fog using diamond-square algorithm. Spatter is a corruption that simulates when an image is wet with water.

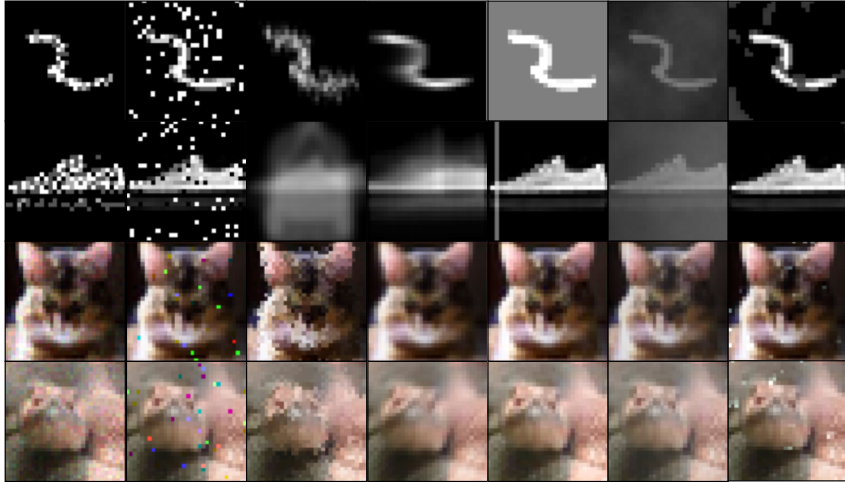


Figure 5: **Seven corruptions.** In eight corruptions, there are shot noise, impulse noise, glass blur, motion blur, brightness, fog, and spatter.

Results of DCGAN[22]. Among the three models evaluated, DCGAN performed the worst. While it achieved a relatively small FID score on the identity dataset, its performance degraded gradually as the dataset became corrupted. DCGAN experienced mode collapse in the presence of impulse noise or shot noise, resulting in repetitive features in generated images. This suggests that the model struggled with the challenges posed by impulse noise and shot noise during training.

Table 4: Results of DCGAN

	Clear	Noise		Blur		Weather		Extra
	identity	impulse	shot	glass	motion	fog	brightness	spatter
MNIST	61.48	251.80	64.25	72.65	105.53	61.54	68.82	101.99
FashionMNIST	46.14	249.99	53.02	125.92	191.63	94.69	51.69	59.35
CIFAR-10	189.13	304.68	190.53	209.24	151.07	189.93	231.99	238.97
CIFAR-100	190.74	228.49	164.11	190.65	195.47	257.49	211.35	244.30

Results of WGAN-GP[23]. Unlike DCGAN, WGAN-GP generated images with diverse features and reduced the performance gap between monochrome and polychrome datasets. However, it still faced challenges in feature extraction and generation when working with corrupted datasets.

Table 5: Results of WGAN-GP

	Clear	Noise		Blur		Weather		Extra
	identity	impulse	shot	glass	motion	fog	brightness	spatter
MNIST	96.40	133.60	95.99	86.61	108.52	140.51	95.51	150.04
FashionMNIST	110.02	136.92	70.64	68.72	128.79	144.12	97.08	99.07
CIFAR-10	126.25	113.48	117.75	113.98	136.57	100.62	119.96	171.68
CIFAR-100	134.46	120.93	153.76	132.79	98.73	94.50	123.13	152.93

B.2 Severity Experiment

In this experiment, we mainly used and analyzed the impact of fog corruptions.

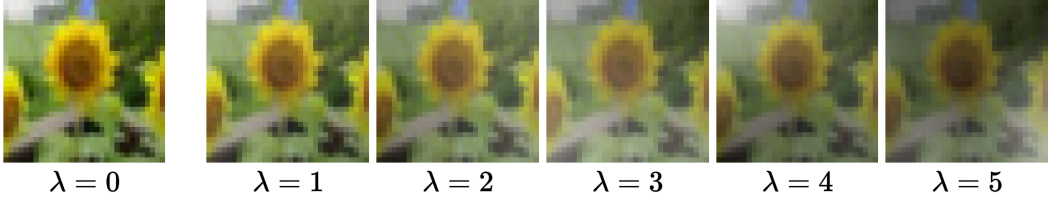


Figure 6: **Image changes with severity.** In this paper, we observed how the performance of DDPM degrades as the severity of the fog corruption increases by varying the severity from 1 to 5.

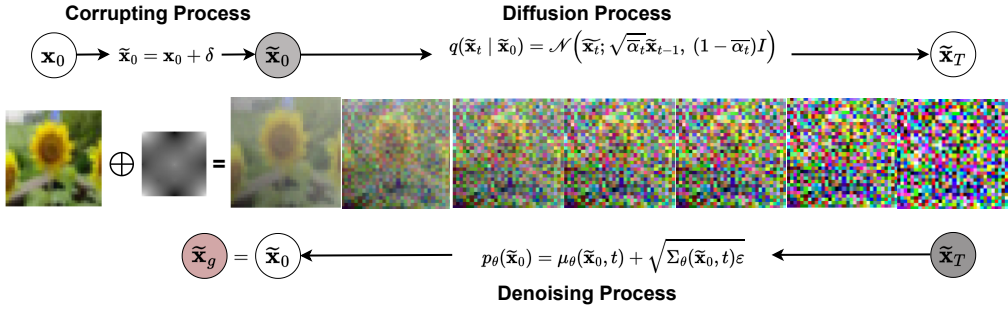


Figure 7: **Mechanism of Diffusion-C used in the Severity Experiments.**

Table 6: FID Scores based on the variations of severity (λ).

	$\lambda = 1$	$\lambda = 2$	$\lambda = 3$	$\lambda = 4$	$\lambda = 5$
MNIST	33.70	16.39	16.30	17.77	24.15
Fashion MNIST	42.80	22.02	24.24	26.82	31.61
CIFAR-10	39.23	37.60	39.07	40.12	38.66
CIFAR-100	44.11	48.41	47.98	48.21	45.15
Tiny-ImageNet	92.88	89.34	85.52	83.15	79.15

B.3 Fractal Independence Experiment

In this experiment, we compared the performance of DDPM between the input as the images added independent fractal corruptions and original fractal images.

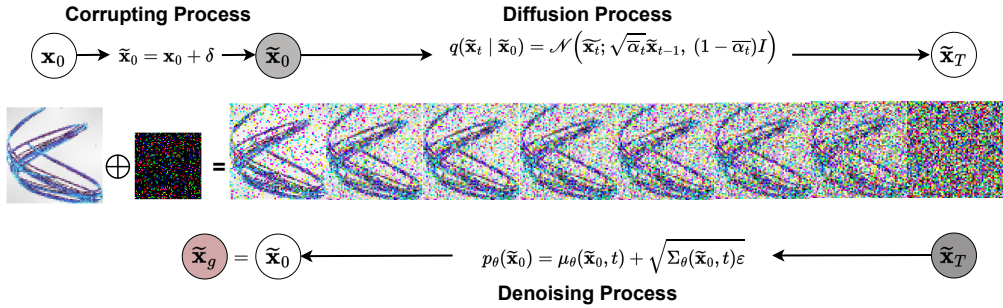


Figure 8: **Mechanism of Diffusion-C used in Fractal Independence experiment.**